Functional Personalization of Patient-Specific Atrial Models Using AF Dominant Frequency

Iris Brahimaj[1], Chiara Celotto[1], Duna De Luis[2], Saman Golmaryami[3], Bettine van Willigen[4], Etel Silva[3], Miguel Rodrigo[2], Elvio Heidenreich[5], Roberto Sassi[6], Massimo Rivolta[6], Joris de Groot[4], José F. Rodriguez Matas[1]

[1] Politecnico di Milano, Milano, Italy
[2] Universitat de València, Valencia, Spain
[3] INiBICA, University Hospital Puerta del Mar, Cádiz, Spain
[4] Amsterdam UMC, Amsterdam, The Netherlands
[6] Università degli Studi di Milano, Milano, Italy

Abstract

The degree of atrial fibrillation (AF)-induced electrical remodeling is usually fixed to a population value in patient-specific atrial models, and in this work we proposed the dominant frequency (DF) as an observable to personalize it. The Courtemanche-Ramirez-Nattel model was remodeled at five levels (0 to 100% of the reference reduction of I_{to}, I_{CaL} and I_{Kur}), over which the wavelength shortened by 13%. Rotors were induced in a 2D sheet for each level combined with 0, 15, 35 and 45% diffuse fibrosis, and in a personalized left atrial model, at three remodeling degrees, three fibrosis configurations and three global conductivities. In 2D, DF rose from 4.71 to 5.59 Hz between 0 and 50% remodeling at 15% fibrosis and then saturated, whereas raising fibrosis to 35% lowered it by 2.3–3.1 Hz and abolished its dependence on remodeling. In the patient model, doubling the remodeling shifted DF by up to 0.34 Hz, one fibrosis level by up to 0.47 Hz in the opposite direction, and a $\pm 20\%$ change of the global conductivity by up to 0.55 Hz without a consistent sign. Reentry sustainability depended far more sharply on the remodeling-fibrosis combination. DF is therefore governed by the structural substrate and by modeling assumptions more than by electrical remodeling.

1. Introduction

Sustained rapid activation during atrial fibrillation (AF) shortens the atrial action potential and refractory period, creating a substrate that favours continued fibrillatory activity [1]. The extent of this electrical remodeling varies across patients and changes with the duration of AF, yet patient-specific models commonly represent it using a fixed population-level value, while geometry, fibrosis and conduction velocity are personalized from clinical data. We have recently shown that structural personalization alone leaves the model weakly constrained by the clinical data, and suggested global functional descriptors as a more promising calibration target [2]. The dominant frequency (DF) is a potential candidate. However, using DF for model calibration requires that it be sufficiently sensitive to the degree of electrical remodeling and distinguishable from the effects of fibrosis and modeling uncertainties. We test those requirements in single cell, in a cable, in a 2D sheet spanning different combinations of remodeling and fibrosis, and in a patient-specific left atrial (LA) model.

2. Methods

2.1. Graded electrical remodeling

Human atrial electrophysiology was described by the Courtemanche-Ramirez-Nattel (CRN) model [3]. Electrical remodeling was reproduced by reducing the maximal conductances of I_{to}, I_{CaL} and I_{Kur} by 50, 70 and 50% (100% remodeling) [4]. Intermediate degrees were obtained by scaling the three reductions by a common factor [5], giving substrates at 0, 25, 50 and 75% of remodeling. The cell, cable and 2D simulations used a generic LA cell, the patient-specific model the region-specific parameterization of [2, 6].

Single cells were paced to steady state at a cycle length of 800 ms. Propagation was simulated in a 2-cm cable ($\Delta x = 0.2$ mm) paced with 100 stimuli. Conduction velocity (CV) was computed from the resulting propagation, while the effective refractory period (ERP) was determined using an S1–S2 protocol (S1 = 100 stimuli at 800 ms) with

a 1-ms resolution. Wavelength (WL) was then calculated as CV $\times$ ERP. All simulations were performed using the monodomain solver ELVIRA [7].

2.2. Rotor frequency in a 2D sheet

Square sheets of 10 cm side were discretized with Δx = 0.2 mm. Fibrosis was introduced by replacing a fraction of the myocytes with MacCannell fibroblasts [8] at randomly selected nodes and reducing the myocyte-fibroblast conductivity by 75%. Four fibrosis densities (0, 15, 35, 45%) were combined with the five remodeling levels. Conductivities were calibrated to a longitudinal CV of 90 cm/s for the non remodeled/non fibrotic case. A rotor was initiated with an S1-S2 cross-field protocol and the simulations were run for a minimum of 2.5 s. A single virtual electrode above the centre of the sheet provided the signals analysed in Section 2.4.

2.3. Patient-specific left atrial model

One patient with persistent AF referred for de novo ablation was included in the prospective, single-centre study conducted at University Hospital Puerta del Mar (Cadiz, Spain), as described in [2]. The study adhered to the Declaration of Helsinki, was approved by the Local Ethics Committee (Protocol SICEIA-2024-001746, Study Code PERSUADE, 03/10/2024), and the participant gave written informed consent. The LA was segmented from pre-procedural computed tomography. Electroanatomical maps were acquired in sinus rhythm (SR), during the triple-extrastimulus (TE) protocol, and during AF, and the surface electrocardiogram (ECG) was recorded simultaneously with the CARTO system.

The segmentation was converted into a tetrahedral mesh and fiber orientations were assigned from an atrial atlas [6]. Baseline conductivities were calibrated to a longitudinal CV of 60 cm/s in the LA, and every configuration was additionally simulated with the global conductivity scaled by $\pm 20\%$ to account for the uncertainty of that calibration [2]. For this patient the nominal and the $+20\%$ values reproduced the clinical activation maps more closely than the -20% one [2], but all three are reported to quantify the sensitivity of DF to CV. Fibrotic regions were derived from the TE bipolar voltage [2], with dense fibrosis below 0.05 mV and moderate fibrosis between 0.05 and 0.5 mV. Inside those regions fibrosis was implemented exactly as in 2D, in three configurations F1–F3 with fibroblast densities of 15/30, 30/50 and 50/75% in moderately and densely fibrotic tissue, plus a baseline diffuse density of 3% elsewhere.

AF was induced with trains of 10 stimuli at the right superior pulmonary vein, and simulations continued for 2.5 s post-induction. A configuration was classified as non-sustained (ns) when the reentry terminated before the end of the simulation, and as non-inducible (ni) when no reentry was established.

2.4. Dominant frequency

The patient AF ECG (1 kHz) was divided into segments free of missing samples, and only segments of at least 30 s were included in the analysis. Ventricular activity was removed with spatiotemporal QRST cancellation [9]. The atrial signal was band-pass filtered between 3 and 9 Hz (fourth-order zero-phase Butterworth), detrended and normalized, and its spectrum estimated over 8 s Hamming-windowed segments overlapping by 75% (resolution 0.12 Hz, smoothed over five bins). DF was defined as the frequency corresponding to the largest peak in the spectrum, averaged across the windows of each segment, in lead aVL, which was selected as the lead that best reflects left atrial activity and therefore provides the most appropriate comparison with the isolated LA model.

Simulated far-field pseudo-ECGs were computed as the extracellular potential generated by the atrial sources in an unbounded homogeneous medium. In the patient model, virtual electrodes were placed at the anatomical positions of the right-arm, left-arm and left-leg electrodes, located 23.8, 23.8 and 45.9 cm from the LA centroid, respectively. Their anatomical directions were reconstructed from the regional labels of the mesh, and lead aVL was computed using the standard Goldberger combination of the three limb-electrode potentials. In the 2D sheet a single virtual electrode was placed 5 cm above the centre of the tissue. Being two orders of magnitude shorter than the clinical recordings, all simulated signals were detrended, tapered with a Tukey window (α = 0.25) and their periodogram computed over the whole record with zero padding, over a band widened to 2–9 Hz.

3. Results

3.1. Cell and cable

Remodeling shortened repolarization monotonically but not proportionally to the scaling factor (Table 1): APD_{90} fell by 17.7% and ERP by 15.6%, with more than a third of the total shortening produced by the last quarter of the range. Both the action potential amplitude (APA) and the maximum upstroke velocity (V_{max}) increased, while the resting membrane potential (RMP) was essentially unchanged. CV increased marginally, so the WL was dominated by refractoriness and decreased by only 13%.

Table 1. Cellular and cable properties as a function of the degree of AF-induced electrical remodeling.

Remodeling	0%	25%	50%	75%	100%
APD_{90} (ms)	204.8	197.9	191.3	182.2	168.5
APA (mV)	102.4	102.7	103.1	103.6	104.1
$\dot{V}_{\max}$ (mV/ms)	204.0	205.7	207.7	209.9	212.2
RMP (mV)	−81.2	−81.1	−81.1	−81.0	−80.9
ERP (ms)	225	219	212	203	190
CV (cm/s)	90.9	91.7	91.7	92.6	93.5
WL (cm)	20.5	20.1	19.4	18.8	17.8

Table 2. DF (Hz) in the 2D sheet. ns: rotor self-terminated after 700–800 ms.

	Fibrosis		
Remod.	0%	15%	35%
0%	4.91	4.71	2.45
25%	5.05	5.15	2.87
50%	ns	5.59	2.52
75%	ns	5.48	2.44
100%	ns	5.52	2.47

3.2. CV and Rotor frequency in 2D

The effect of remodeling on CV depended on the fibrotic substrate: over the whole remodeling range CV increased by 2% at both 0 and 15% fibrosis, but decreased by 14% at 35%. Whether the rotor was sustained depended on the combination of the two factors. Without fibrosis it persisted for the whole simulation only at 0 and 25% remodeling and self-terminated after 700–800 ms at 50, 75 and 100%; with 15 and 35% fibrosis it persisted at every remodeling level; at 45% the tissue was not conductive. The trajectory of the phase singularity (Fig. 1) illustrates this behaviour: without fibrosis the rotor meandered around a limited region at 0% remodeling but drifted across the sheet at 50 and 100%, whereas with 15% fibrosis the trajectory remained confined at every remodeling level. At 15% fibrosis, where all five substrates sustained the arrhythmia, DF increased from 4.71 Hz in control to 5.59 Hz at 50% remodeling and then stopped, so that the whole range spans 0.88 Hz and only its lower half carries information Fibrosis moved DF considerably more and in the opposite direction. Raising the density from 15 to 35% lowered DF at every remodeling level, by 2.26 and 2.28 Hz at 0 and 25% and by 3.04–3.07 Hz at 50, 75 and 100%, up to three and a half times the range spanned by remodeling. At 35% the rotor became wide and slow and DF lost its dependence on remodeling altogether, the five values ranging non-monotonically between 2.44 and 2.87 Hz. From 0 to 15% fibrosis, in contrast, DF changed by less than 0.2 Hz, so the transition occurs between 15 and 35%.

3.3. Patient-specific model

Reentry was induced and sustained only in a subset of the 27 configurations, and the subset depended on the combination of remodeling and fibrosis rather than on either separately (Table 3). At 0% remodeling only F1 sustained the arrhythmia; at 50 and 100% the opposite occurred, F1 being non-inducible while F2 and F3 sustained reentry. Reducing the conductivity by 20% terminated the reentry in three of the four remodeled configurations in which it was otherwise sustained. Where a comparison at fixed fibrosis and conductivity was possible, doubling the remodeling from 50 to 100% raised DF by 0.05, 0.34 and 0.20 Hz, whereas raising the fibrosis configuration by one level lowered it by 0.29, 0.47 and 0.43 Hz, about twice as much and in the opposite direction. The $\pm 20\%$ conductivity variation shifted DF by up to 0.55 Hz, more than the effect of remodeling and without a consistent sign. The highest DF of the whole set was 5.25 Hz, at 0% remodeling, and all remodeled configurations lay between 3.74 and 4.49 Hz, below the 6.31 Hz measured in the patient.

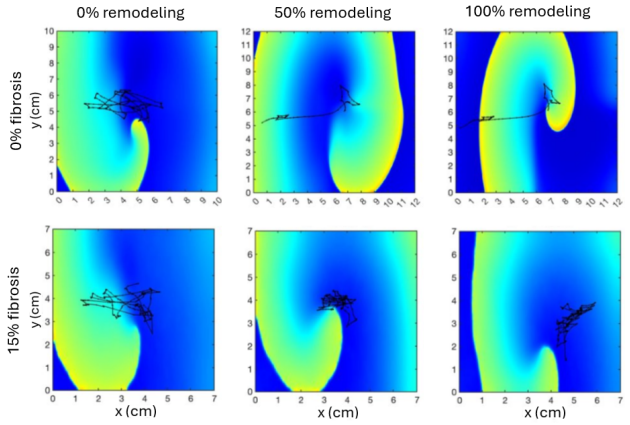

Figure 1. Trajectory of the phase singularity (black) over a snapshot of the transmembrane potential, for 0% (top) and 15% (bottom) fibrosis at three degrees of remodeling.

Table 3. Simulated DF (Hz) in the patient-specific model, reported as σ nominal / $+20\%$ / -20%. F1–F3: fibroblast densities of 15/30, 30/50 and 50/75% in moderately and densely fibrotic tissue. ns: reentry not sustained; ni: not inducible.

Remodeling	F1	F2	F3
0%	5.25 / 4.70 / 5.22	ns	ns
50%	ni	4.17 / 4.15 / 4.09	ns / 3.86 / ns
100%	ni	4.21 / 4.49 / ns	3.74 / 4.06 / ns

4. Discussion

In both the 2D sheet and the patient model, DF was far more sensitive to fibrosis and to the conductivity assumption than to electrical remodeling, and at high fibrosis density it lost any dependence on remodeling at all. DF therefore reports more on the structural substrate than on the ionic remodeling it was meant to identify, and under these

conditions the inversion is poorly constrained: the voltage-derived fibrosis map carries its own uncertainty [2], and the parameter the calibration should identify is the one to which the observable is least sensitive.

These contrasting effects of remodeling and fibrosis arise from their different mechanisms. Remodeling shortens refractoriness but also raises the amplitude and upstroke velocity of the action potential, making the tissue more excitable; fibrosis instead affects propagation, slowing conduction, lengthening the route of the wavefront, and partially depolarizing myocytes coupled to fibroblasts. This explains both observations. The frequency saturates because, once the reentry develops an excitable gap, further shortening of refractoriness no longer accelerates it, whereas at high fibrosis density the cycle length is set by the circuit rather than by tissue properties. Sustainability, in turn, requires the rotor to keep a functional block region to rotate around: increased excitability lets the wavefront invade it, so that without fibrosis the rotor drifted until it reached the boundary (Fig. 1), while the heterogeneities introduced by fibrosis anchored it. Each remodeling level therefore required a minimum fibrosis density, increasing with remodeling, and whereas frequency differed between these configurations by a few tenths of a hertz, inducibility separated them completely.

Finally, no simulated configuration reached the DF measured in the patient. Two scenarios may account for this. First, the real remodeling may be more severe than the reference condition adopted here, which does not include the upregulation of I_{K1} reported in persistent AF [10]; including it would shorten refractoriness further and widen the range of attainable frequencies. Second, the model represents the LA alone, whereas the surface ECG reflects the activity of both atria. Other limitations should be considered. First, a single ionic model and a single definition of AF-induced remodeling were considered; a population-of-models approach would establish whether the limited identifiability found here is a property of DF itself or of this particular parameterization. Second, the analysis is based on one patient, and additional cases are being processed for a future publication. Finally, reentry was induced from a single pacing site, so that a configuration classified as non-inducible might sustain reentry if initiated elsewhere.

5. Conclusions

DF carried information on remodeling only at low fibrosis density; as fibrosis increased, the cycle length came to be governed by the reentrant circuit and the dependence on remodeling vanished. DF therefore appears of limited use for identifying the degree of electrical remodeling in the fibrotic substrates typical of persistent AF, whereas the inducibility and sustainability of the reentry discriminated between substrates more clearly and may deserve attention as a complementary calibration target.

Acknowledgments

Supported by the ERA4Health Partnership, the European Union through Horizon Europe under Grant Agreement 101095426, ERA4HEALTH CVD-124 PERSUADE, and the Spanish Ministry of Science under Grant PCI2024-153442.

References

[1] Wijffels MC, Kirchhof CJ, Dorland R, Allessie MA. Atrial fibrillation begets atrial fibrillation. *Circulation* 1995;92:1954–1968.

[2] Celotto C, de Luis D, Golmaryami S, et al. Probing atrial substrate with the triple extrastimulus protocol: impact of variability on electrophysiological metrics. *IEEE Trans Biomed Eng* 2026;73(8):2922–2939.

[3] Courtemanche M, Ramirez RJ, Nattel S. Ionic mechanisms underlying human atrial action potential properties. *Am J Physiol* 1998;275:H301–H321.

[4] Courtemanche M, Ramirez RJ, Nattel S. Ionic targets for drug therapy and atrial fibrillation-induced electrical remodeling. *Cardiovasc Res* 1999;42:477–489.

[5] Krogh-Madsen T, Abbott GW, Christini DJ. Effects of electrical and structural remodeling on atrial fibrillation maintenance: a simulation study. *PLoS Comput Biol* 2012;8(2):e1002390.

[6] Ferrer A, Sebastián R, Sánchez-Quintana D, et al. Detailed anatomical and electrophysiological models of human atria and torso for the simulation of atrial activation. *PLoS One* 2015;10:e0141573.

[7] Heidenreich EA, Ferrero JM, Doblaré M, Rodríguez JF. Adaptive macro finite elements for the numerical solution of monodomain equations in cardiac electrophysiology. *Ann Biomed Eng* 2010;38:2331–2345.

[8] MacCannell KA, Bazzazi H, Chilton L, et al. A mathematical model of electrotonic interactions between ventricular myocytes and fibroblasts. *Biophys J* 2007;92:4121–4132.

[9] Stridh M, Sörnmo L. Spatiotemporal QRST cancellation techniques for analysis of atrial fibrillation. *IEEE Trans Biomed Eng* 2001;48(1):105–111.

[10] Bosch RF, Zeng X, Grammer JB, et al. Ionic mechanisms of electrical remodeling in human atrial fibrillation. *Cardiovasc Res* 1999;44:121–131.

Address for correspondence:

Chiara Celotto
Politecnico di Milano, Piazza Leonardo da Vinci 32, 20133 Milan, Italy
chiara.celotto@polimi.it